THE ASTROPHYSICAL JOURNAL, 530:371–386, 2000 February 10


# RADIO CONTINUUM EMISSION AT OH AND $H_2O$ MASER SITES

J. R. FORSTER
University of California, Berkeley, and Hat Creek Radio Observatory, 42231 Bidwell Road, Hat Creek, CA 96040; rforster@astron.berkeley.edu
AND
J. L. CASWELL
Australia Telescope National Facility, Commonwealth Scientific and Industrial Research Organization, PO Box 76, Epping, NSW 2121, Australia
*Received 1999 May 14; accepted 1999 September 27*

## ABSTRACT

A search for centimeter radio continuum emission associated with OH and $H_2O$ masers has been made toward 26 fields containing 45 separate maser sites using the Australia Telescope Compact Array (ATCA) at 8.2 and 9.2 GHz. The sensitivity achieved for fields not limited by dynamic range is $\sim$0.15 mJy rms. This is the deepest radio search for embedded stellar sources at sites containing OH and $H_2O$ masers made to date. Only 17 compact continuum sources were detected within 2″ of the 45 maser sites searched. The absence of 3 cm continuum emission at the mJy level in 62% of the maser sites shows that most OH/$H_2O$ maser sites do not contain well-developed ultracompact H II regions (UCHIIs). The implications of this result on the nature of the source pumping the maser emission are discussed. While other possibilities cannot be ruled out, we argue that many maser sites without detected UCHIIs are most likely massive stars still in the pre–main-sequence contraction stage.

*Subject heading:* H II regions — masers — stars: pre–main-sequence

## 1. INTRODUCTION

Since the discovery of OH masers nearly 35 years ago (Weaver et al. 1965) evidence has accumulated linking OH and $H_2O$ masers to massive young stars and ultracompact H II regions (UCHIIs). Most pumping models rely on an embedded young stellar object (YSO) to provide the excitation energy for maser action (Cook 1968; Elitzur & de Jong 1978; Tarter & Welch 1986; Baart & Cohen 1985). Little is certain regarding the nature of the object or objects responsible for maser excitation, however. For example, the mass limit of stars capable of producing maser radiation and the evolutionary stage of the stars during the maser phase are unknown.

A high detection rate (67%) of $H_2O$ masers in a search toward known UCHIIs by Churchwell, Walmsley, & Cesaroni (1990) added support to the idea that OB stars are the exciting source for both OH and $H_2O$ masers. However, accurate position measurements showed that the masers are often not coincident with H II regions and that many maser sites do not have obvious H II counterparts. The detection of HCN emission at the position of the $H_2O$ maser group $\sim$7″ east of the UCHII W3(OH) (Turner & Welch 1984) was the first example of an isolated water maser located in a massive molecular clump. This raised the possibility that the embedded YSO is protostellar, an idea originally suggested by Mezger & Robinson (1968) for OH masers.

While observations of interstellar masers and their environments continue to improve, many measurements essential for a better understanding of the maser process and its relationship to massive star formation are still not available. For example, data on the size and mass of molecular clumps at maser sites are available for only a few sources (Turner & Welch 1984; Cesaroni et al. 1994), and little is known about the overall mass and dust distribution in these sources.

At the early stage of star formation in which masers are produced a central exciting star or star cluster is difficult to detect. Observation at optical wavelengths is impossible because of heavy obscuration by dust. Instruments capable of providing both high sensitivity and high resolution in the far-infrared (FIR) or submillimeter are still in their infancy, and emission from warm dust at these wavelengths is a source of confusion. An indirect way of detecting massive stars is to search for their radio continuum emission. Free-free radiation from the ionized zone produced by embedded stars of type B0.5 or earlier should be detectable at centimeter wavelengths over most of the Galaxy. For example, a spherical H II region at a distance of 10 kpc with a radius of 10 mpc ($3.1 \times 10^{16}$ cm), an electron density of $10^5$ cm$^{-3}$, and a temperature of $10^4$ K produces a flux density of 25 mJy at 8 GHz. This corresponds to a zero-age main-sequence (ZAMS) star of spectral type B0 (Panagia 1973).

Most detections of H II regions at maser sites have been made as adjuncts to molecular line studies, e.g., those of Forster & Caswell (1989, hereafter FC89), Caswell (1997, hereafter C97), Codella, Testi, & Cesaroni (1997), and Ellingsen, Norris, & McCullough (1996). Tofani et al. (1995) have done the deepest search to date, following up observations of 22 $H_2O$ masers associated with molecular outflows with VLA observations of the continuum at 8.4 GHz. Carral et al. (1999) searched for 3.6 cm continuum emission toward 12 luminous *IRAS* sources, several containing OH, $H_2O$, or $CH_3OH$ sites. Recent attempts to directly observe the YSO responsible for maser activity have concentrated on individual sources associated with $H_2O$ masers and molecular outflows (Hofner et al. 1999; Marti, Rodriguez, & Torrelles 1999; Torrelles et al. 1997, 1998). No observations have been made specifically to search for continuum emission at a large number of sites containing both OH and $H_2O$ masers. Such a search, made using a substantially complete and unbiased sample, could provide useful constraints on the nature of the YSOs powering interstellar OH and $H_2O$ masers.

This paper reports the results of a deep search toward 45 maser sites in 26 fields containing both OH and $H_2O$ masers using the Australia Telescope Compact Array

(ATCA) at 3 cm wavelength. The 26 fields are from the FC89 survey, restricted to sources with Galactic longitudes in the range 352°.52–24°.79. The fields observed form an essentially complete sample of sites known to contain both maser species in this part of the Galaxy, although several fields containing strong continuum sources that have already been studied extensively were omitted (5.88−0.39, 10.62−0.38 and 15.03−0.68). The purpose of this survey is to provide sensitive measurements of any compact 3 cm radio continuum emission at the locations of known OH and $H_2O$ maser sites. The primary aim is to improve our understanding of interstellar maser sources, in particular, to learn more about the objects responsible for maser excitation.

## 2. OBSERVATIONS AND DATA REDUCTION

The ATCA observations were made in seven 10 hr sessions during the period 1997 November 26–December 2. Four fields were observed each day by alternately observing each field for 2 minutes, followed by a 2 minute calibration on a nearby QSO. The time interval between successive phase calibrations was about 20 minutes. Daytime weather conditions were clear and hot with strong afternoon winds. Phase variation caused by atmospheric turbulence was substantial on the longer baselines. Atmospheric decorrelation is estimated to be about a factor of 1.57 for most sources. Primary flux calibration was based on an assumed flux density of 3.0 Jy for the compact extragalactic source 1934−638.

Orthogonal polarizations at two frequencies centered at 8.256 and 9.152 GHz were observed simultaneously, with 128 MHz bandwidth received in each polarization and each frequency (i.e., the effective instantaneous bandwidth was 512 MHz). System temperatures were typically 45 K near the zenith and 60 K at 20° elevation. Individual integration times were 20 s for each visibility measurement. The primary beam of the 22 m AT antennas is ∼5′.7 FWHM at 9 GHz.

The six-element ATCA was used in its most extended configuration, providing 15 baselines ranging from 180 to 6000 m (6 to 185 k$\lambda$). Spatial filtering severely reduced the sensitivity to sources larger than about 10″. Owing to the rather sparse UV coverage, large-scale structure was not well imaged and tended to raise the rms noise level in the maps. For this reason short UV spacings were omitted when extended sources were present. Synthesized beams were ∼1″.3 in right ascension and 1″.3/sin (decl.) in declination with natural weighting. The sensitivity achieved was ∼0.15 mJy beam$^{-1}$ (1 $\sigma$) in fields not limited by dynamic range. The dirty images were cleaned using the Hogbom algorithm and restored with a 1″.5 FWHM circular Gaussian beam. The circular restoring beam was used to eliminate the artificial elongation in declination caused by the east-west orientation of the array and to simplify the calculation of spectral indices from the measured flux densities at the two observing frequencies.

The data were calibrated and imaged using the MIRIAD reduction package (Sault, Teuben, & Wright 1995). Total intensity (Stokes I) maps 3′.4 on a side were produced at each frequency. This size was sufficient to cover all known maser sources in each field observed. Calibration, mapping, and analysis were performed separately for each frequency in order to allow the spectral index of detected continuum sources to be derived. Gaussian fits were made to the detected compact sources to obtain an estimate of the total flux density and size of the UCHIIs.

Self-calibration was used to reduce atmospheric decorrelation and improve the dynamic range for fields that contained sufficient flux. The initial calibration using nearby QSOs provided a good starting model for self-calibration, so no position information is lost by using this procedure. Self-calibration was found to increase the peak flux density measured for compact sources by a factor of about 1.2 for a self-calibration interval of 2 minutes and up to a factor 2.4 for a 1 minute interval. The median increase for all self-calibratable fields was a factor 1.57. For fields that were not self-calibrated, the true point-source sensitivity is therefore estimated to be about a factor of 1.57 worse than the value derived from the image statistics.

## 3. RESULTS

Continuum images for each field observed are shown in Figure 1. The contours represent the average intensity of the combined 8.2 and 9.2 GHz images. The 100 mpc linear scale bar is based on a Galactic center distance of 10 kpc for consistency with FC89. If the currently accepted value of 8.5 kpc (Kerr & Lynden-Bell 1986) is used, the scale bar represents a linear size of 85 mpc. The OH and $H_2O$ maser positions are accurate to ∼0″.5 rms, although the relative positions between maser spots of the same species are better determined (Forster & Caswell 1999). Given the combined positional uncertainty of the continuum peaks and maser spots and the typical extents of the maser groups and continuum sources, any maser spot within 2″ of a continuum peak is considered to be associated with it. In view of the large number of maser sites observed in this survey, we do not expect position errors to significantly affect the results.

Table 1 lists each observed field center and the maser sites present in the field (far right column), along with the UCHII detections. Within each field a UCHII is referred to by a label ("A," "B," "C," etc.) to locate it easily on the maps, followed by its full source name (Galactic coordinates cited to millidegree precision, as used in the Becker et al. 1994 Galactic plane catalog). The angular distance to an OH or $H_2O$ maser is given when it is regarded as associated (i.e., separation less than 2″). The spectral index listed is derived from the peak rather than the total flux density because the peaks and their uncertainties are better defined than the total fluxes. There is generally good consistency between the spectral index determined either way. The uncertainty in the spectral index was estimated using flux density ratios altered by adding the rms in the numerator and subtracting in the denominator. The quoted uncertainty in peak flux density is the rms value measured directly from image statistics and does not include atmospheric decorrelation. For fields containing strong sources the rms is dominated by dynamic range effects. For other fields the rms is determined by system noise. Fields for which no UCHII was detected are listed at the bottom of the table.

The strong UCHIIs detected in this survey correspond to previously known sources in many cases. For example, two sources from Garay, Reid, & Morgan (1985) and two from Caswell (C97; Caswell 1998) were detected, and six detections from the FC89 survey have been confirmed. Three reported detections from FC89 (359.14+0.03, 359.62−0.25, and 12.91−0.26) that were not confirmed are now believed to be spurious. FC89 used spectral channels thought to be free of $H_2O$ maser emission to produce their continuum

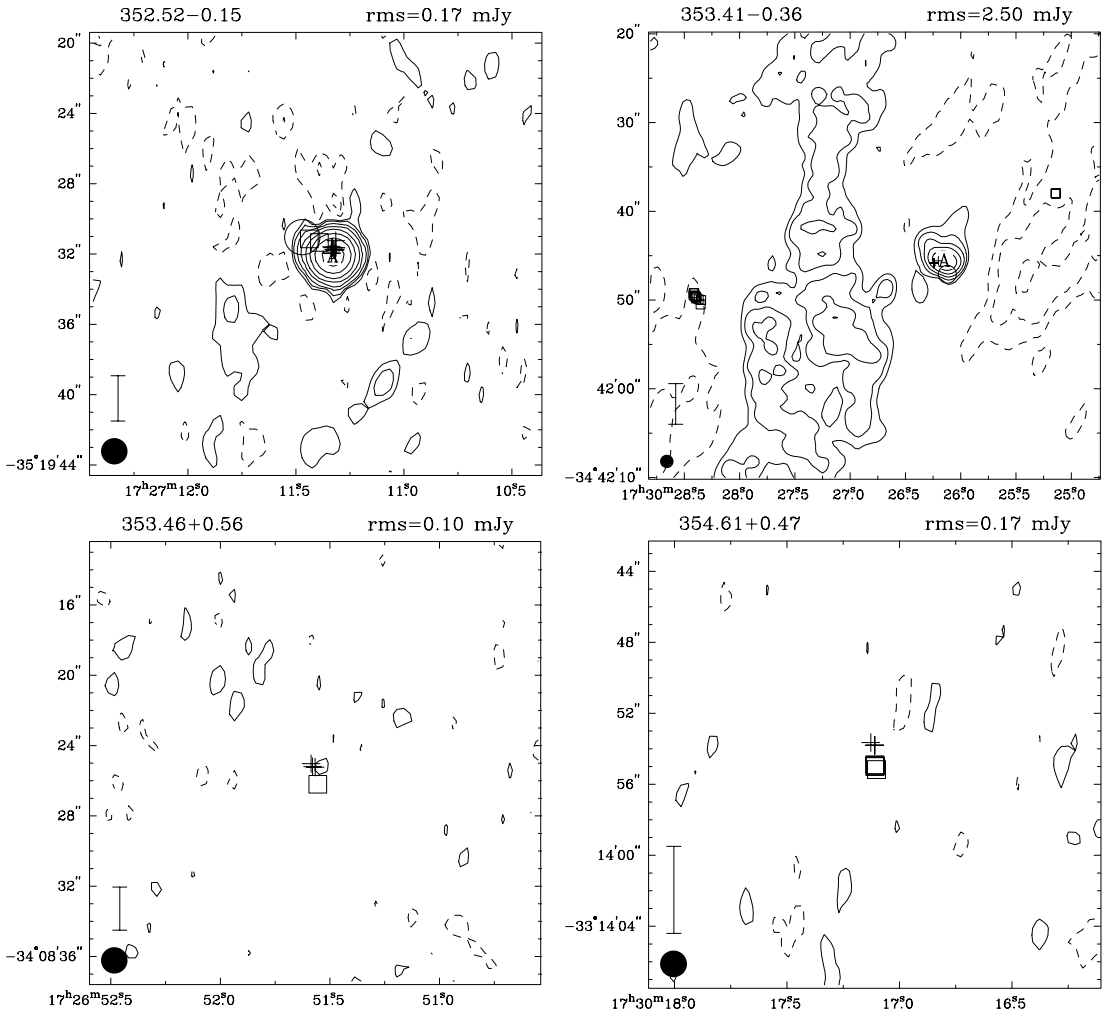


FIG. 1.—Three cm $\lambda$ continuum contours are shown, starting at 2 $\sigma$ and doubling with each successive contour (2 $\sigma$, 4 $\sigma$, 8 $\sigma$, ...). The rms (1 $\sigma$) level is given at the top of each plot. The peak positions of detected UCHIIs are marked by capital letters; full Galactic source names are given in Table 1. OH masers, $H_2O$ masers, and 22 GHz VLA continuum detections from Forster & Caswell (1999) are indicated by crosses, open squares, and circles respectively. The 1.″5 circular restoring beam and a 100 mpc linear scale bar are shown in the lower left-hand corner. The linear scale assumes the distances listed in Table 1, which are based on a Galactic center distance of 10 kpc. RA and decl. coordinates are for equinox 2000.0.

maps; the spurious detections may be due to contamination by $H_2O$ lines not evident in their scalar-averaged spectra. Counterparts to our UCHIIs in the Becker et al. (1994) survey (at lower frequency and resolution) sometimes correspond to a blend of more than one UCHII, as discussed in the individual source notes.

The total number of maser sites present in all fields combined is 45. These consist of 20 simple maser associations (defined as overlapping groups of OH and $H_2O$ masers with extent $\lesssim$30 mpc), 16 isolated $H_2O$ masers (without overlapping OH counterparts), and nine isolated OH masers. Of the 45 maser sites present, 17 (38%) coincide with compact continuum sources. UCHIIs were detected in 10 (50%) sites containing both OH and $H_2O$ masers, in five (56%) of the isolated OH maser groups, and in two (13%) of the isolated $H_2O$ groups in our sample.

The total number of UCHIIs detected in all fields combined is 29, of which 17 (59%) are associated with masers. Thus the high detection rate of masers at the locations of known H II regions noted by Churchwell et al. (1990) is confirmed. The converse also holds for OH masers, but not for $H_2O$ masers. 52% of the maser sites containing OH have UCHIIs. For sites containing $H_2O$ masers the overall UCHII detection rate is 33%. Most of these $H_2O$ sites also contain OH masers; for isolated $H_2O$ masers (without OH counterparts) the detection rate is much lower (13%).

The results from Table 1 are summarized in Figure 2. The top four panels show histograms of total flux density and angular size for the detected continuum sources. The angular size plotted is the geometrical mean radius obtained from the deconvolved source size ($R = (\Theta_{maj}\,\Theta_{min})^{1/2}/2$). UCHIIs with associated masers are shown in gray. The distributions adjusted to a fixed distance of 5 kpc (4.25 kpc for a Galactic center distance of 8.5 kpc) are given in the right-hand column. The total flux histograms show that most UCHIIs in our sample have flux densities below 75 mJy. The total flux adjusted to a distance of 5 kpc shows a strong peak below 25 mJy, composed mainly of UCHIIs with maser emission. Sources without maser emission appear more evenly distributed in flux density than those with masers. The distribution of angular sizes on the sky shows that most UCHII radii are $\lesssim$2″. UCHIIs without maser emission tend to be larger than those with masers. Adjusted to a distance of 5 kpc, the nonmaser

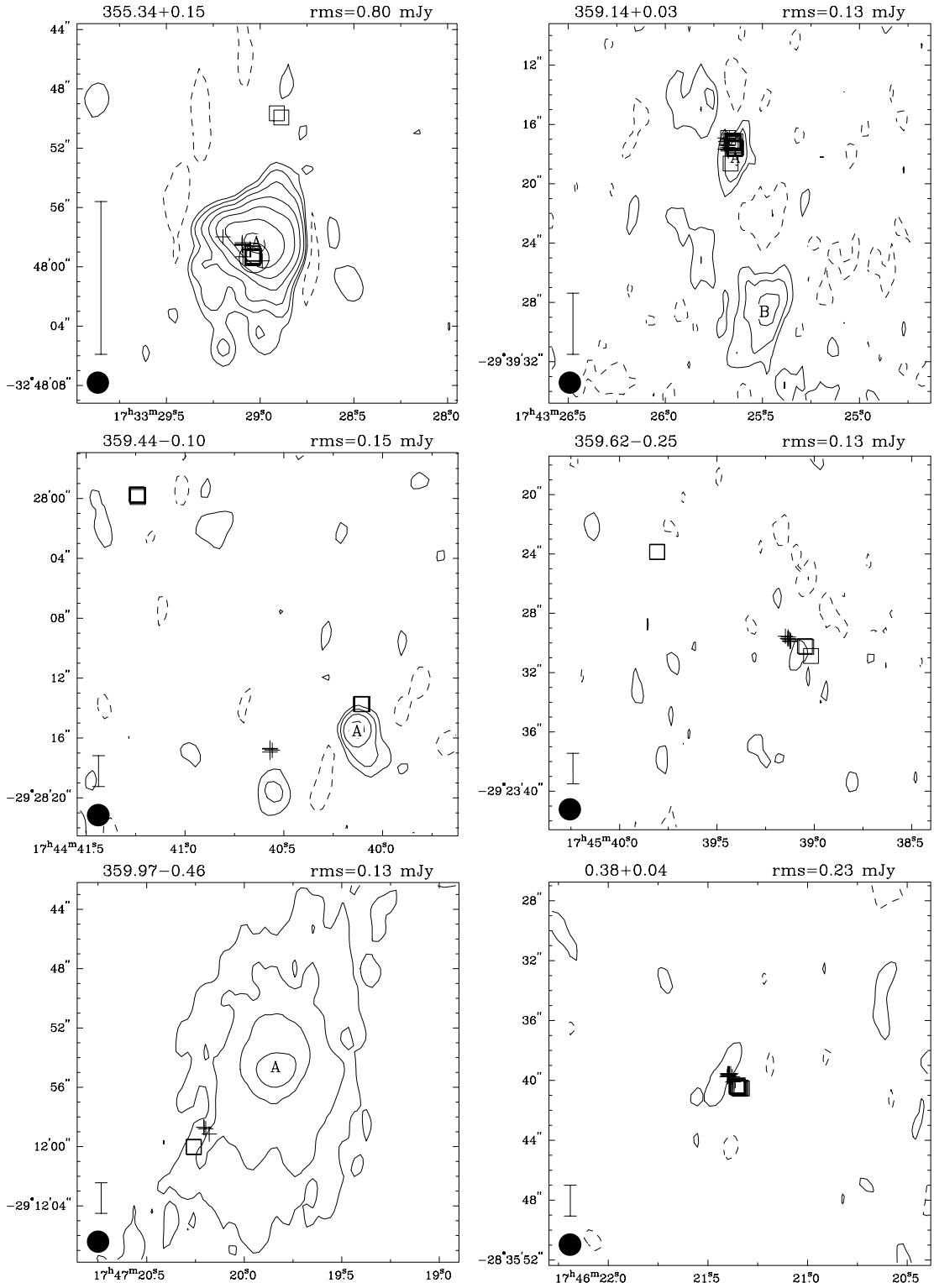


FIG. 1.—*Continued*

sources are fairly evenly distributed over sizes $\gtrsim 0\farcs5$, while UCHIIs associated with masers are concentrated in the region $\lesssim 1''$ (24 mpc). This histogram also shows that most of the UCHIIs detected in this survey have radii less than 30 mpc.

The bottom two panels in Figure 2 show the spectral index derived from the peak flux densities measured at 8.2 and 9.2 GHz. Since the spectral index depends only on the flux ratio, it is independent of distance. The histogram shows that the majority of UCHIIs have slightly positive spectral indexes (0–0.4) and that the distributions for maser and nonmaser sources are similar. Most sources with negative spectral index are consistent within the errors with a flat or slightly positive spectrum. The left-hand panel plots the spectral index versus measurement uncertainty, with the maser associations indicated by filled circles. From this plot it can be seen that the best determined values lie between 0 and 1.0 and are mostly UCHIIs associated with masers.

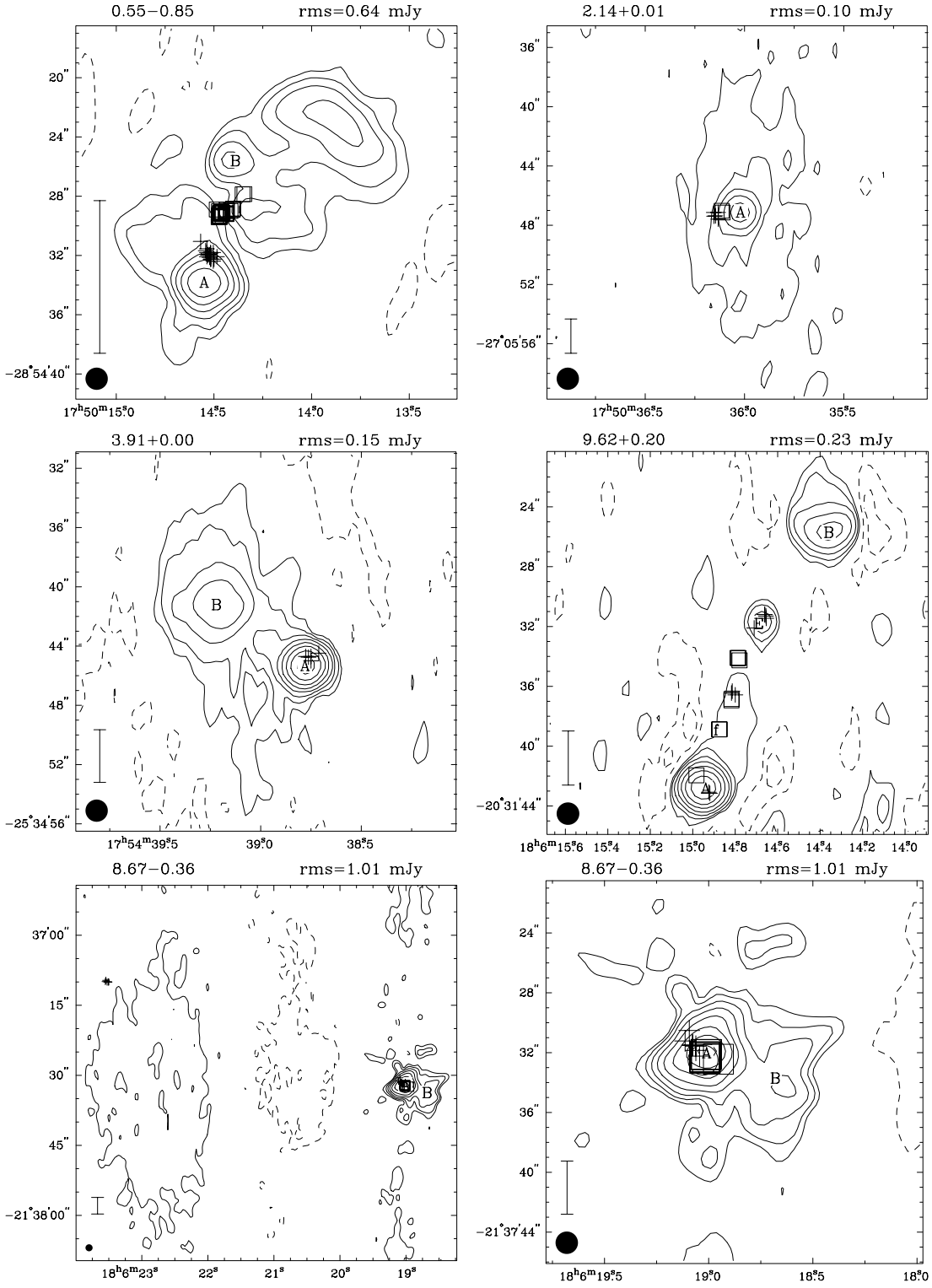


FIG. 1.—*Continued*

The implications of these results are discussed in the next section. Comments on individual sources follow. Some readers may prefer to skip to the discussion (§ 4) and return to this section as needed.

*352.52−0.15*—A barely resolved UCHII is coincident with a simple OH/$H_2O$ maser association. A 7 k$\lambda$ UV cutoff was used to eliminate large-scale emission that appears to surround the UCHII, and the finally measured flux density of 73 mJy was 1.56 larger than before the application of self-calibration. FC89 reported an 80 mJy source at 22.2 GHz, offset about 2″ northwest from our peak position. Becker et al. (1994) reported 30.6 mJy at 5 GHz. Caswell (1998) found 53 mJy at 6.7 GHz, and a $CH_3OH$ maser coincident with the OH. The data below 22 GHz are consistent with a spectral index of $\sim$0.9.

*353.41−0.36*—A resolved UCHII is coincident with an isolated OH maser in this field. Two isolated $H_2O$ masers without UCHIIs are located $\sim$30″ east and 17″ northwest

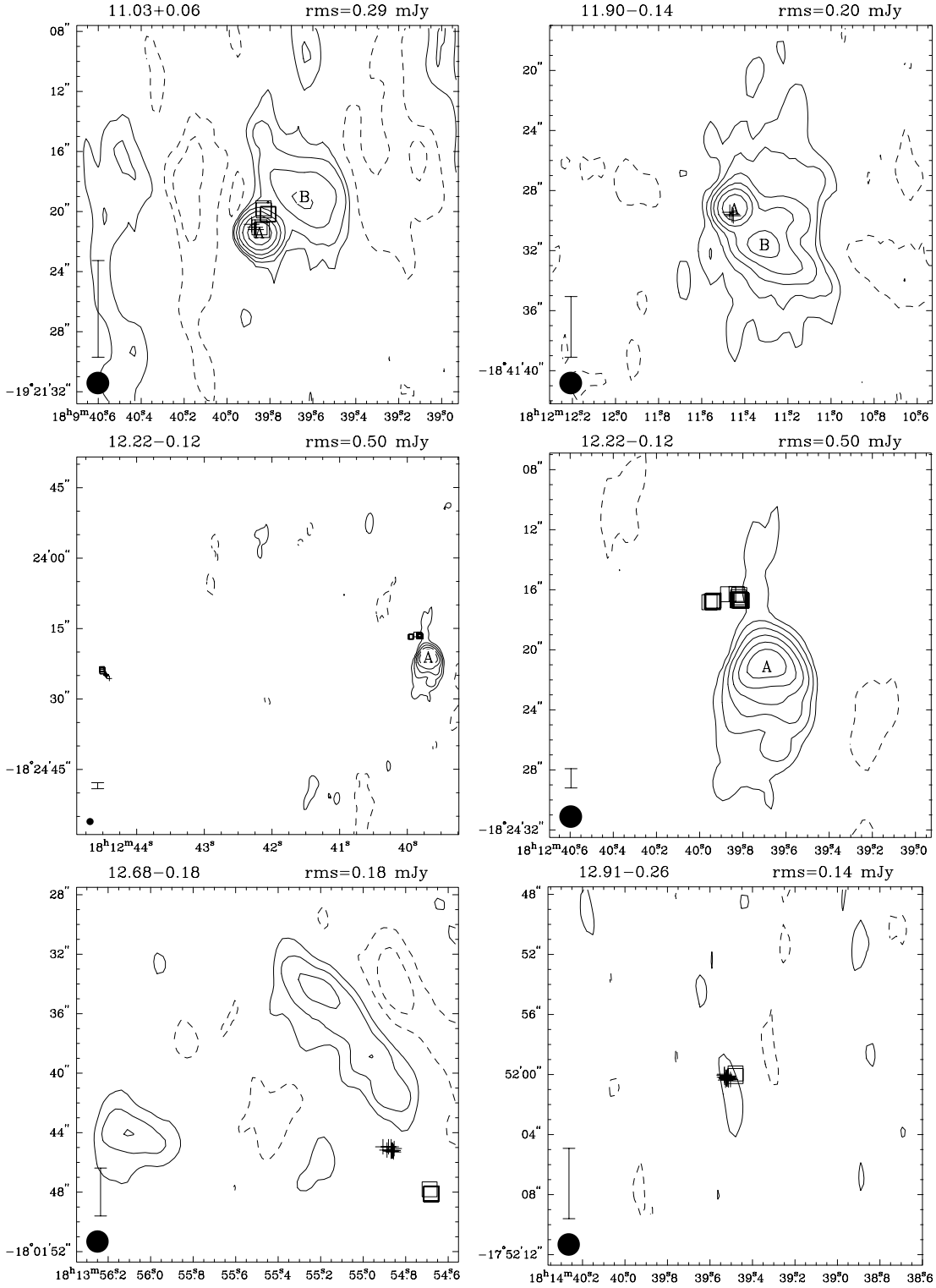


FIG. 1.—*Continued*

of the OH group. Several Jy of extended emission is also present, which appears in Figure 1 as an elongated structure located between the UCHII and the eastern $H_2O$ maser. A 520 mJy H II region located 2″ southeast of our position was reported by FC89. Gaume & Mutel (1987) report a 15 GHz peak flux density of 270 mJy beam$^{-1}$ and C97 found a peak flux density of 315 mJy beam$^{-1}$ and a total flux of 800 mJy at 6.7 GHz, while Becker et al. (1994) at 5 GHz list peak and integrated values of 118 and 214 mJy. Our peak and integrated fluxes at 9 GHz are 215 mJy beam$^{-1}$ and 415 mJy beam$^{-1}$ after application of self-calibration (which led to a factor 1.56 increase). Despite small inconsistencies, the data are generally compatible with a fairly flat high-frequency spectral index, as expected from thermal emission optically thin at 9 GHz. C97 finds 6 GHz $CH_3OH$ and excited OH masers coincident with the UCHII. The map shows no UCHIIs detected at the locations of the two isolated water masers to an rms limit of 2.5 mJy. The large amount of

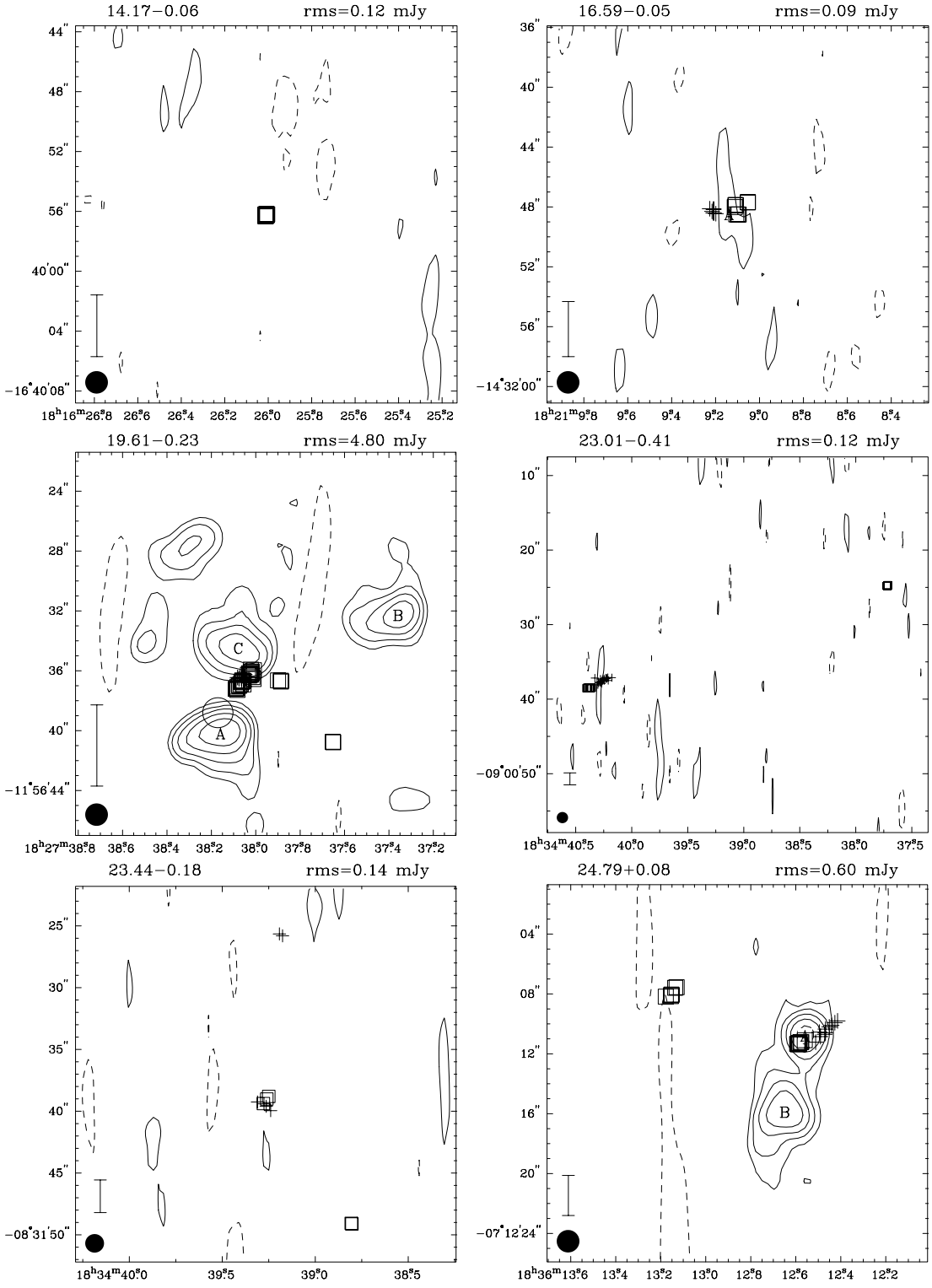


FIG. 1.—*Continued*

extended flux in the region is responsible for the high noise level in the map and for some of the discrepancies among different surveys. If more of the large-scale structure is filtered from our map, the noise level is reduced and additional possible compact sources are seen. One of these is a 14 mJy source at RA = $17^h30^m28^s.55$, decl. = $-34°41'49''.2$, which is within 2″ of the eastern $H_2O$ maser site. This source is located in a depressed region caused by dynamic range limitations in the map shown in Figure 1, and therefore does not appear in that image. We have not listed these uncertain sources in Table 1 pending confirmation observations, but the occurrence of matching features on a 15 GHz map by Gaume & Mutel (1987) suggests that they are most likely genuine sources of size less than 1″. If they are UCHIIs, the detection statistics toward isolated $H_2O$ masers would be slightly changed from 2/16 to 3/16.

*353.46+0.56*—No continuum emission was detected in this field to an rms limit of 0.10 mJy (0.16 with estimated

TABLE 1

ULTRACOMPACT H II REGIONS

| FIELD CENTER[a] (l, b) | UCHII[b] LABEL | UCHII NAME (l, b) | UCHII POSITIONS (J2000) RA | UCHII POSITIONS (J2000) decl. | D[c] (kpc) | PEAK[d] (mJy beam$^{-1}$) | H II SIZE[e] (arcsec) | TOTAL[f] (mJy) | SPECTRAL INDEX[g] | OFFSET[h] $H_2O$ | OFFSET[h] OH | MASER SITES PRESENT[i] |
|---|---|---|---|---|---|---|---|---|---|---|---|---|
| 352.52−0.15..... | A | G352.518−0.155 | 17 27 11.33 | −35 19 32.1 | 8.0 | 66.7 ± 0.2 | 0.5 × 0.4 | 73.4 | 0.94 ± 0.1 | 1.1 | 0.4 | S |
| 353.41−0.36..... | A | G353.410−0.360 | 17 30 26.15 | −34 41 45.5 | 4.5 | 203.4 ± 2.5 | 2.1 × 1.2 | 415.1 | −0.14 ± 0.3 | ... | 0.6 | OH, 2$H_2O$ |
| 355.34+0.15..... | A | G355.344+0.147 | 17 33 29.02 | −32 47 58.3 | 2.0 | 124.7 ± 1.0 | 3.3 × 2.5 | 524.4 | 0.15 ± 0.2 | 0.5 | 0.2 | S, $H_2O$ |
| 359.14+0.03..... | A | G359.137+0.031 | 17 43 25.64 | −29 39 18.2 | 5.0 | 1.3 ± 0.1 | Point | 1.3 | −2.65 ± 2.7 | 0.5 | 0.7 | S |
| | B | G359.135+0.030 | 17 43 25.49 | −29 39 28.6 | 5.0 | 1.2 ± 0.1 | 4.4 × 2.0 | 6.2 | −4.02 ± 2.8 | ... | ... | ... |
| 359.44−0.10..... | A | G359.436−0.102 | 17 44 40.13 | −29 28 15.5 | 10.0 | 3.2 ± 0.2 | 1.4 × 0.3 | 4.3 | 1.22 ± 1.2 | 1.8 | ... | OH, 2$H_2O$ |
| | B | G359.425−0.111 | 17 44 40.55 | −29 29 04.0 | 10.0 | 5.5 ± 0.2 | Point | 5.7 | −0.44 ± 0.7 | ... | ... | ... |
| 359.97−0.46..... | A | G359.970−0.456 | 17 47 19.84 | −29 11 54.6 | 10.0 | 4.1 ± 0.1 | 3.6 × 3.0 | 18.6 | 0.09 ± 0.8 | ... | ... | S |
| 0.55−0.85 ..... | A | G0.546−0.852 | 17 50 14.55 | −28 54 33.8 | 2.0 | 80.1 ± 0.6 | 1.7 × 1.6 | 167.4 | 0.25 ± 0.2 | ... | 1.8 | OH, $H_2O$ |
| | B | G0.548−0.851 | 17 50 14.39 | −28 54 25.6 | 2.0 | 13.1 ± 0.6 | 2.7 × 2.0 | 35.6 | 0.15 ± 2.5 | 2.0 | ... | |
| 2.14+0.01 ..... | A | G2.143+0.009 | 17 50 36.02 | −27 05 47.1 | 8.9 | 4.9 ± 0.1 | 1.5 × 1.1 | 7.5 | 0.18 ± 0.5 | 1.4 | 1.5 | S |
| 3.91+0.00 ..... | A | G3.911+0.001 | 17 54 38.78 | −25 34 45.3 | 5.8 | 53.4 ± 0.2 | 0.7 × 0.5 | 64.4 | 0.51 ± 0.1 | ... | 0.6 | OH |
| | B | G3.912−0.000 | 17 54 39.22 | −25 34 41.2 | 5.8 | 3.8 ± 0.2 | 3.8 × 3.6 | 26.9 | 0.10 ± 1.0 | ... | ... | ... |
| 8.67−0.36 ..... | A | G8.669−0.356 | 18 06 19.01 | −21 37 32.0 | 5.8 | 322.0 ± 1.0 | 2.1 × 1.6 | 711.2 | 0.27 ± 0.1 | 0.4 | 0.6 | S, OH |
| | B | G8.668−0.355 | 18 06 18.68 | −21 37 33.7 | 5.8 | 19.8 ± 1.0 | 6.0 × 4.3 | 195.0 | 0.34 ± 1.1 | ... | ... | ... |
| 9.62+0.20 ..... | A | G9.619+0.193 | 18 06 14.94 | −20 31 42.8 | 5.7 | 54.2 ± 0.3 | 0.7 × 0.6 | 66.5 | 0.77 ± 0.2 | 1.0 | 0.4 | 2S, OH, 2$H_2O$ |
| | B | G9.622+0.197 | 18 06 14.36 | −20 31 25.7 | 5.7 | 9.9 ± 0.3 | 2.2 × 1.6 | 23.6 | −0.17 ± 1.2 | ... | ... | ... |
| | E | G9.621+0.195 | 18 06 14.68 | −20 31 31.7 | 5.8 | 3.0 ± 0.3 | Point | 3.4 | 0.00 ± 2.0 | ... | 0.5 | |
| 11.03+0.06..... | A | G11.034+0.061 | 18 09 39.85 | −19 21 21.4 | 3.2 | 36.3 ± 0.3 | 0.6 × 0.4 | 40.9 | 0.37 ± 0.2 | 0.5 | 0.5 | S |
| | B | G11.034+0.062 | 18 09 39.64 | −19 21 19.0 | 3.2 | 5.3 ± 0.3 | 4.6 × 2.8 | 31.6 | −1.80 ± 1.5 | ... | ... | ... |
| 11.90−0.14..... | A | G11.904−0.142 | 18 12 11.45 | −18 41 29.2 | 5.1 | 28.6 ± 0.2 | 0.9 × 0.6 | 33.9 | 0.64 ± 0.1 | ... | 0.4 | OH |
| | B | G11.903−0.141 | 18 12 11.31 | −18 41 31.6 | 5.1 | 10.9 ± 0.2 | 2.6 × 1.6 | 29.1 | 0.18 ± 0.4 | ... | ... | ... |
| 12.22−0.12..... | A | G12.208−0.102 | 18 12 39.69 | −18 24 21.1 | 16.1 | 61.4 ± 0.5 | 2.3 × 1.8 | 163.8 | 0.00 ± 0.2 | ... | ... | S, $H_2O$ |
| 16.59−0.05..... | A | G16.585−0.051 | 18 21 09.14 | −14 31 48.5 | 5.6 | 0.3 ± 0.1 | Point | 0.3 | −0.40 ± 5.0 | 0.8 | 0.6 | S |
| 19.61−0.23..... | A | G19.609−0.236 | 18 27 38.16 | −11 56 40.2 | 3.8 | 319.0 ± 4.8 | 2.3 × 1.3 | 699.0 | 0.88 ± 0.3 | ... | ... | S, 2$H_2O$ |
| | B | G19.609−0.232 | 18 27 37.36 | −11 56 32.3 | 3.8 | 138.2 ± 4.8 | 1.8 × 1.0 | 274.5 | −0.70 ± 0.7 | ... | ... | ... |
| | C | G19.610−0.235 | 18 27 38.08 | −11 56 34.5 | 3.8 | 124.2 ± 4.8 | 2.8 × 1.5 | 375.5 | 0.08 ± 0.8 | 2.0 | 2.0 | |
| 24.79+0.08..... | A | G24.790+0.083 | 18 36 12.56 | −7 12 10.8 | 7.7 | 26.3 ± 0.6 | 1.1 × 0.7 | 36.2 | 2.08 ± 0.5 | 0.4 | 0.7 | S, $H_2O$ |
| | B | G24.789+0.082 | 18 36 12.65 | −7 12 15.9 | 7.7 | 20.3 ± 0.6 | 2.1 × 1.8 | 51.2 | −0.29 ± 0.6 | ... | ... | ... |
| Fields in Which No UCHIIs Were Detected[j] | | | | | | | | | | | | |
| 353.46+0.56..... | ... | ... | 17 26 52.00 | −34 08 25.0 | 8.4 | ±0.1 | ... | ... | ... | ... | ... | S |
| 354.61+0.47..... | ... | ... | 17 30 17.11 | −33 13 56.9 | 4.2 | ±0.2 | ... | ... | ... | ... | ... | S |
| 359.62−0.25..... | ... | ... | 17 45 39.00 | −29 23 30.0 | 10.0 | ±0.1 | ... | ... | ... | ... | ... | S, 2$H_2O$ |
| 0.38+0.04 ..... | ... | ... | 17 46 21.34 | −28 35 42.6 | 10.0 | ±0.2 | ... | ... | ... | ... | ... | S |
| 12.68−0.18..... | ... | ... | 18 13 54.68 | −18 01 48.1 | 6.4 | ±0.2 | ... | ... | ... | ... | ... | OH, 2$H_2O$ |
| 12.91−0.26..... | ... | ... | 18 14 39.48 | −17 52 00.1 | 4.4 | ±0.1 | ... | ... | ... | ... | ... | S |
| 14.17−0.06..... | ... | ... | 18 16 26.01 | −16 39 56.2 | 5.0 | ±0.1 | ... | ... | ... | ... | ... | $H_2O$ |
| 23.01−0.41..... | ... | ... | 18 34 40.39 | −9 00 40.5 | 12.8 | ±0.1 | ... | ... | ... | ... | ... | S |
| 23.44−0.18..... | ... | ... | 18 34 39.25 | −8 31 40.8 | 7.8 | ±0.1 | ... | ... | ... | ... | ... | S, OH, $H_2O$ |

NOTE.—Units of right ascension are hours, minutes, and seconds, and units of declination are degrees, arcminutes, and arcseconds.

[a] For brevity the field centers are referenced by their Galactic coordinates without the acronym G.

[b] Letter designation for detected UCHIIs (see maps).

[c] Kinematical distance based on a Galactic center distance of 10 kpc.

[d] Peak flux density of the best-fitting Gaussian derived from the combined 8.2 and 9.2 GHz images.

[e] Major and minor axes in arcseconds of the fitted Gaussian source.

[f] Total flux density of the fitted Gaussian source.

[g] Spectral index $\alpha$ ($S \sim \nu^{\alpha}$) derived from the ratio of peak intensities at 8.2 and 9.2 GHz.

[h] Offset to the nearest OH or $H_2O$ maser spot in arcsec. No entry implies that no corresponding maser exists within 2″ of the continuum position.

[i] Maser sites present in the field: S contains both OH and $H_2O$ masers at the same location; OH is an isolated OH maser group; 2$H_2O$ indicates two isolated $H_2O$ maser sites in the field.

[j] Positions listed are the field centers. Peak flux limits are 1 $\sigma$.

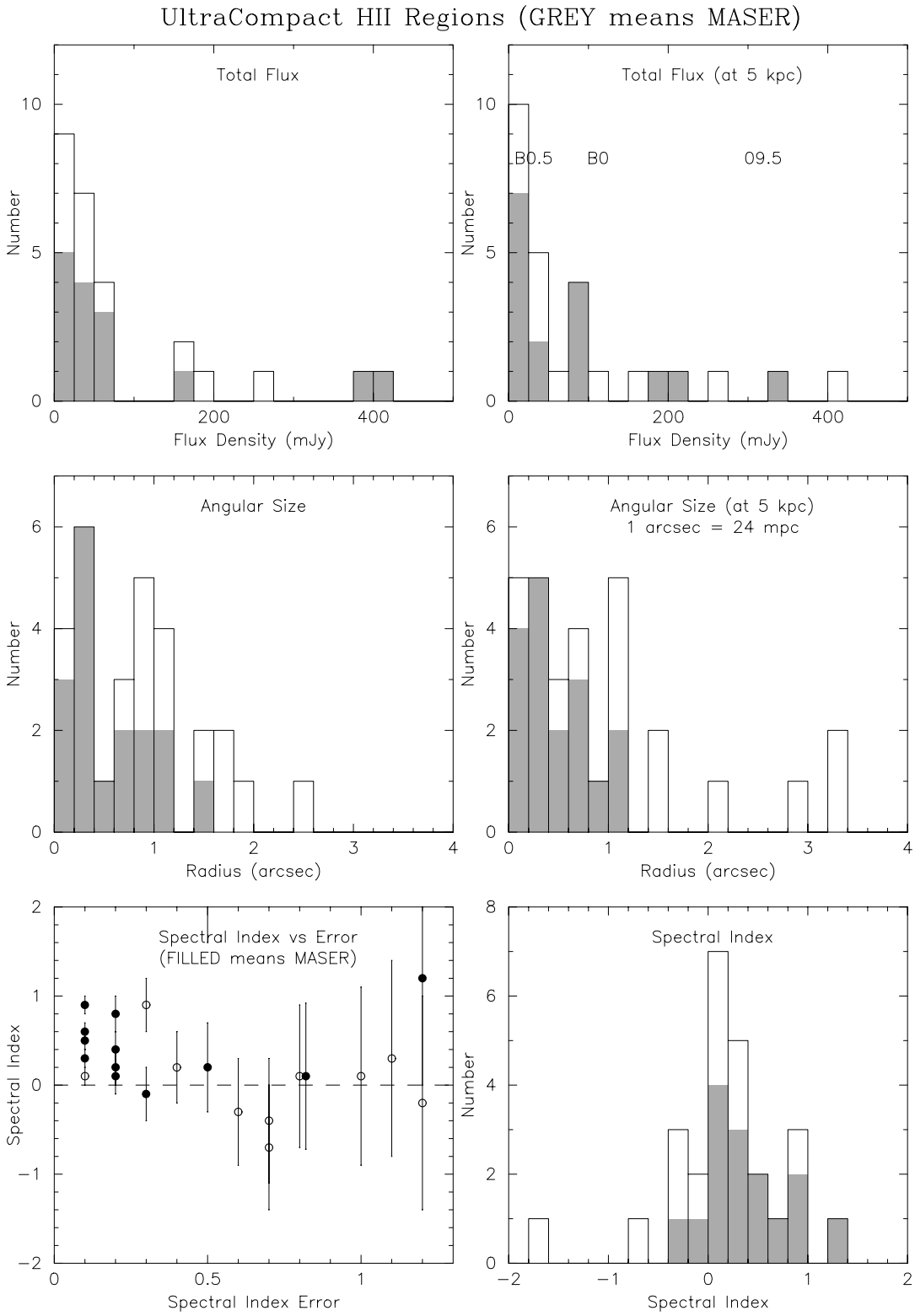


FIG. 2.—*Top panels*: Distribution of total flux. *Right panel*: Adjusted for a 5 kpc distance, with the fluxes corresponding to several stellar spectral types indicated. *Middle panels*: Distribution of H II radii in arcsec (*left panel*) as measured and (*right panel*) adjusted to $D = 5$ kpc. *Bottom panels*: Spectral index plotted against (*left panel*) the measurement error and (*right panel*) the spectral index distribution. Shaded areas of the histograms and filled symbols indicate UCHIIs that are associated with maser sites.

decorrelation). A 7 k$\lambda$ UV cutoff was used to reduce the effect of extended emission detected at a level of $\sim$0.2 Jy beam$^{-1}$. A $CH_3OH$ maser is coincident with the simple OH/$H_2O$ association.

*354.61+0.47*—No continuum was detected to a level of 0.17 mJy rms (0.27 with decorrelation) near the simple OH/$H_2O$ group in this field. Several extended sources located $\sim$3′ northeast and 0.7′southwest contaminate the

image. Using a UV cutoff of 20 k$\lambda$ removed most of this emission. A $CH_3OH$ maser lies within a few arcsec of the OH maser (Caswell, Vaile, & Forster 1995).

*355.34+0.15*—A well-resolved UCHII is found coincident with a simple $OH/H_2O$ maser group and 22 GHz continuum source. $CH_3OH$ and excited OH masers are also associated with the $OH/H_2O$ group. FC89 list a 150 mJy source at a position 1″ south of our peak; C97 measure 570 mJy total and 160 mJy beam$^{-1}$ peak flux density at 6.7 GHz; Becker et al. (1994) measure 341 mJy total and 240 mJy beam$^{-1}$ peak flux density at 5 GHz. Our 9 GHz flux density is 125 mJy beam$^{-1}$ peak and 524 mJy total (after self-calibration, which led to a 1.40 factor increase). Despite some disparities the available data are accounted for by a fairly flat spectral index. An isolated $H_2O$ group is located 9″ north of the UCHII. This maser also coincides with a $CH_3OH$ maser. No continuum is detected to an rms level of 0.8 mJy at this location. The high noise level near the H II region is due to dynamic range limitations.

*359.14+0.03*—A 1.3 mJy unresolved UCHII (A) is detected at the location of the simple $OH/H_2O$ group in this field. $CH_3OH$ and excited OH are also found at this position (C97). A more extended H II region (B) is located 11″ south. B is reported by Becker et al. (1994) with similar integrated flux density (4.9 mJy), but A is below their sensitivity limit. Extended emission, possibly associated with source B, required use of a UV cutoff at 5 k$\lambda$. Since this field could not be reliably self-calibrated, the flux densities quoted may be underestimated by as much as a factor of 2. Note on FC89: a 530 mJy continuum source was reported at the maser position. This must be a spurious detection, possibly because of contamination by $H_2O$ emission, since such a bright UCHII would produce much more flux density than we detect at 9 GHz.

*359.44−0.10*—A 4.3 mJy source (A) is detected 1.″8 south of an isolated $H_2O$ maser. Another isolated $H_2O$ maser lies ~20″ northeast, and an isolated OH maser (with an associated $CH_3OH$ maser) lies ~7″ southeast of UCHII A. There is a 0.8 mJy (4 $\sigma$) peak 3″ south of the OH maser, but contamination by strong extended emission nearby suggests that this may be an artifact. A 20 k$\lambda$ UV cutoff was used to minimize the problem, but the strength of the contamination and our inability to self-calibrate this data urges caution. An unresolved 6 mJy source (B) lies ~50″ south of A (not shown in the figure). The only close (within 2″) association between UCHIIs and maser sources in this field is UCHII A and the southern $H_2O$ maser.

*359.62−0.25*—No continuum was detected to a limit of 0.13 mJy rms in this field. The presence of extended emission required a UV cutoff of 7 k$\lambda$. A $CH_3OH$ maser coincides with the simple $OH/H_2O$ association, and an isolated $H_2O$ maser is located ~12″ northeast. Note on FC89: a 70 mJy continuum source was reported ~5″ southwest of the $OH/H_2O$ group. This is close to the sensitivity limit of FC89 and is probably spurious since there is no evidence of it in our data.

*359.97−0.46*—An extended H II region is found 7″ northwest of a simple $OH/H_2O$ maser group (also $CH_3OH$). The H II region has a peak of 4.1 mJy beam$^{-1}$ (after a 1.23 factor increase from self-calibration) and a core size of ~3″. Its large size suggests that it is probably too evolved to be directly related to the masers.

*0.38+0.04*—No continuum was detected near the simple $OH/H_2O$ group (also with $CH_3OH$) in this field to an rms limit of 0.23 mJy. A complex spherical source 30″ in diameter was found ~90″ to the east (not shown in the figure). Contamination by this source was reduced by using a UV cutoff of 14 k$\lambda$.

*0.55−0.85*—Several continuum sources are detected in this field, which contains OH, $H_2O$ and $CH_3OH$ masers clustered within a few arcseconds. More than 1 Jy of continuum emission was detected in this field; using a UV cutoff of 7 k$\lambda$ eliminated about one- half of the flux, and self-calibration increased point source flux densities by a factor of 1.21. Two compact sources are identified, although source B may be a density condensation within an extended shell H II region. FC89 classify this maser association as a simple $OH/H_2O$ group, although the separation between the OH and $H_2O$ masers is about 2″. The OH masers are within 2″ of source A, which makes their association likely. The $H_2O$ masers are nearer to B, with the closest maser spot 2″ from the peak of the continuum emission. The small condensation directly west of the $H_2O$ maser group appears to be part of the larger H II region and is therefore not considered a candidate UCHII. We therefore tentatively associate the $H_2O$ maser group with source B.

*2.14+0.01*—A compact UCHII with an extended halo is found ~1.″5 east of a simple $OH/H_2O$ group (with $CH_3OH$). The total flux density of the slightly resolved core is 7.5 mJy (after a self-calibration increase by a factor of 1.17). Becker et al. (1994) list this source with a 5 GHz flux density of 5.2 mJy.

*3.91+0.00*—Two UCHIIs are found in this field. The stronger and more compact source (A) is coincident with an isolated OH maser (also $CH_3OH$). The weaker H II region (B) 7″ northeast of A is not associated with any known maser. The total flux density of the stronger component is 64 mJy at 9 GHz (after a self-calibration increase by a factor 1.58). The 6.7 GHz flux is 45 Jy (Caswell 1998). Becker et al. (1994) list both sources, but with lower flux densities at 5 GHz.

*8.67−0.36*—There are two maser groups in this field separated by ~1′ east-west. An 80″ field is included in Figure 1 in order to show both maser sites. The eastern site contains an isolated OH maser group (also $CH_3OH$) located near a low surface brightness (2 mJy beam$^{-1}$) region of very large extent but no compact features. The extended emission disappears if a UV cutoff of 7 k$\lambda$ is used, and self-calibration increased the flux densities by a factor of 1.61. The western maser site consists of a simple $OH/H_2O$ association (with $CH_3OH$) coincident with the peak of an extended 711 mJy UCHII (A). Another extended H II region (B) is located 5″ southwest with a total flux density of 195 mJy. The stronger source is cataloged by Becker et al. (1994).

*9.62+0.20*—This interesting field contains a string of maser sites extending 13″ in a north-northwest direction. Although it is difficult to be sure which maser groups are independent and which are related, we consider the string to consist of two simple $OH/H_2O$ associations, two isolated $H_2O$ groups, and one isolated OH group. $CH_3OH$ masers are also present near the southern $OH/H_2O$ association (source A in the figure) and the northern isolated OH maser (UCHII E). The field is confused by a large (20″ diameter) H II region located 13″ west of UCHII A. Emission from this source has been largely eliminated from our image by using a UV cutoff of 20 k$\lambda$. Self-calibration increased the flux densities of compact features by a factor of 2.28. The

continuum image is limited by dynamic range, probably because of the complexity and amount of extended structure in this field. The southernmost OH/$H_2O$ group coincides with UCHII A, and the northern OH maser with UCHII E. No masers are located at the position of UCHII B. There is weak emission at two of the other maser sites, but this may be caused by the limited dynamic range. Becker et al. (1994) list just A and B, at 5 GHz, with similar flux densities. On the other hand, a 2.7 mm source (Hofner et al. 1996) is located at the position marked "f," which coincides with an isolated $H_2O$ maser. Although $H_2O$ was not detected by FC89 at site E, Hofner & Churchwell (1996) list a $H_2O$ maser at that position. This is also the location of an $NH_3$ maser (Hofner et al. 1994), and of the strongest 6.6 GHz $CH_3OH$ maser known in the Galaxy (Caswell 1998). Note on FC89: according to Hofner et al. (1994) the distance to this source is 5.7 kpc.

*11.03+0.06*—Two compact sources are detected in this field, which also contains substantial extended emission. Self-calibration increased the flux densities by a factor of 2.28. A barely resolved 41 mJy UCHII (A) is coincident with a simple OH/$H_2O$ association. The more extended source (B) may be a density enhancement within a much larger H II region, which has been mostly eliminated by using a UV cutoff of 14 k$\lambda$. A single source is cataloged by Becker et al. (1994) at 5 GHz, and is probably a blend dominated by the more diffuse UCHII (B).

*11.90−0.14*—Two compact sources are detected, both of which are embedded in an extended halo of low surface brightness. Self-calibration increased the flux densities by a factor 2.42. An isolated OH maser (with $CH_3OH$) coincides with a slightly resolved 34 mJy UCHII (A). No masers are found near the more extended 29 mJy source (B) located 3″ southwest of A. C97 finds 38 mJy at 6.0 GHz for UCHII A and 25 mJy for B. A source listed by Becker et al. (1994) at 5 GHz is a blend of these two sources. The flux density ratios from our 8 and 9 GHz data suggests that both sources are moderately optically thick, in agreement with the 6.0 GHz flux density for source B but not for A. Note on FC89: a misprint for the reference position of the OH source occurred in FC89. The correct position (Forster & Caswell 1999) agrees with the excited OH position of C97 and with UCHII A.

*12.22−0.12*—This field contains an isolated $H_2O$ maser (with $CH_3OH$) and an OH/$H_2O$ association located 75″ east. An 80″ field is included in Figure 1 in order to show them both. The eastern OH/$H_2O$ site has no methanol or H II region associated with it. A cometary H II region is located near the western $H_2O$ maser. Becker et al. (1994) catalog the source at 5 GHz with flux density 167 mJy, approximately the same as at 9 GHz. The peak of this extended H II region is more than 4″ from the $H_2O$ group. The presence of substantial extended emission in the field required a UV cutoff of 7 k$\lambda$, but image quality is still limited by dynamic range or confusion effects. Self-calibration increased the flux densities of compact features by a factor of 1.83. The tongue of emission extending north from the H II region contains a weak source near the $H_2O$ maser group, but this is not considered a detection because of its weakness and the limited dynamic range. A large distance (16.1 kpc) is assumed for this source. However, the extent of both the H II region and the maser groups in the field suggests that it may be much nearer.

*12.68−0.18*—This area contains at least 0.5 Jy of emission located near the field center and extending over 30″. A UV cutoff of 14 k$\lambda$ was used in the imaging, which eliminated most of this emission and resulted in an rms level of $\sim$0.2 mJy. The continuum map shows several extended sources, which are probably small-scale structure related to the extended emission and not UCHIIs. There are no UCHIIs located near the OH and $H_2O$ maser groups (also $CH_3OH$) in this field. Note on FC89: an ATCA check of the OH position shows it to be closer to the $H_2O$ position than shown in Figure 1 but still $\sim$2″ away from it.

*12.91−0.26*—Contamination from a large source at the $\sim$1 Jy level affects the sensitivity in this field. A UV cutoff of 18 k$\lambda$ gives an rms of 0.14 mJy in the resulting image. We do not claim a continuum detection at the position of the simple OH/$H_2O$ group (with $CH_3OH$), although a 2.5 $\sigma$ peak coincides with it. Note on FC89: the 80 mJy continuum detection reported is not confirmed and is probably spurious.

*14.17−0.06*—Extended emission at the 0.1 Jy level is mostly eliminated using a UV cutoff of 5 k$\lambda$, resulting in a measured rms of 0.12 mJy. There is no UCHII located at the position of the isolated $H_2O$ maser in this field, nor was $CH_3OH$ detected there.

*16.59−0.05*—A very weak (0.3 mJy) UCHII is found coincident with the simple OH/$H_2O$ association in this field. A 5 k$\lambda$ cutoff was used to reduce the effect of a weak halo surrounding this source. Although the UCHII is only a little over 3 $\sigma$, we believe it is a real detection because it is the brightest source in both the 8 and 9 GHz maps.

*19.61−0.23*—This field contains over 4 Jy of flux density, consisting of at least 4 compact sources embedded in several Jy of extended emission. A UV cutoff of 14 k$\lambda$ was used to lower the background level and reduce confusion. Self-calibration gave an increase in peak flux density by a factor of 1.46, but dynamic range limitations raise the effective noise level near the H II regions to an rms of 4.8 mJy. We identify three sources that we believe are UCHIIs. Source A is about 4″ southeast of an OH/$H_2O$ association and close to the 22 GHz continuum source listed in FC89. Source C is within 2″ of the OH/$H_2O$ masers and may therefore be considered associated with it. Source B is not near any known masers. In the image made using full UV coverage the two eastern sources appear as part of a ridge of emission extending toward the south. While these might be UCHIIs they could also be density enhancements in an extended H II region and therefore are not listed as UCHIIs in Table 1. The two isolated $H_2O$ sources southwest of UCHII C have no associated continuum sources but coincide with $NH_3$ clumps mapped by Garay et al. (1998). Garay et al. (1985) have done detailed studies of this region in the continuum and in recombination lines. Our UCHII labels have been chosen to correspond to their nomenclature, which follows the original notation of Ho & Haschick (1981). Becker et al. (1994) list a single complex of 11.″4 extent.

*23.01−0.41*—Several extended sources contaminate this field, but most of this emission is eliminated using a UV cutoff of 20 k$\lambda$. There is a 0.37 mJy (3.1 $\sigma$) feature coincident with the simple OH/$H_2O$ group (also $CH_3OH$). We do not consider this a detection however since there are several other features in the field that are as large. There is no continuum near the isolated $H_2O$ maser located $\sim$40″ west of the OH/$H_2O$ association.

*23.44−0.18*—There are three well-separated maser sites in this field, but no associated continuum sources are

detected to a level of 0.14 mJy rms. There is a slightly resolved 6 mJy source located $\sim 1'.5$ northeast of the field center (RA = $18^h34^m44^s.92$, decl. = $-8°31'07''.8$), which is not listed in Table 1 or shown in the figure. A 7 k$\lambda$ UV cutoff was required to eliminate nearly 1 Jy of contaminating flux. The simple OH/$H_2O$ association near the field center also contains $CH_3OH$.

*24.79+0.08*—Two slightly resolved UCHIIs are detected. UCHII A is coincident with a simple OH/$H_2O$ association (with $CH_3OH$). UCHII B does not have any associated maser emission. The isolated $H_2O$ maser $\sim 9''$ northeast of component A does not have any detectable continuum emission. We detected nearly 2 Jy of flux from an extended source in the field, most of which is eliminated by using a UV cutoff of 10 k$\lambda$. Self-calibration increased the flux densities of small diameter features by a factor of 1.64. Codella et al. (1997) show a similar map of the region from VLA observations at 23.7 GHz. The total flux density measured at 8.2, 9.2 and 23.7 GHz suggests that UCHII A is optically thick at 9 GHz and turns over somewhere between 9 and 23 GHz, which would account for its absence from the Becker et al. (1994) catalog at 5 GHz. The opacity of UCHII B is substantially less than A, and it is cataloged by Becker et al. (1994) at 5 GHz with flux density 32 mJy.

## 4. DISCUSSION

The absence of detected continuum sources at more than half of the maser sites is perhaps the most interesting result of this survey. Our continuum detection rate of 38% is in general agreement with the rates found by Caswell (C97) and Tofani et al. (1995) in surveys conducted toward, respectively, 6 GHz OH masers, and 22 GHz $H_2O$ masers associated with molecular outflows. The low detection rate is difficult to explain if masers are excited by embedded ZAMS OB-type stars, which should produce easily detectable H II regions. Heavy extinction of the UV by dust within the H II region (Wood & Churchwell 1989), or an extremely small size would reduce the detectability of the ionized zone around a massive star. Extreme youth for the embedded YSO might also account for the absence of continuum emission (Codella et al. 1994; Codella, Felli, & Natale 1996). If a massive stellar core is present but still in the protostellar collapse stage, the YSO may be energetic enough to excite maser emission but not hot enough to produce an ionized zone. Similarly, if the embedded star has a spectral type later than B1 or B2, insufficient UV is available to produce a detectable H II region. Finally, if the masers are excited by an external source no continuum emission is expected at the maser site itself. In this section the following explanations for the low continuum levels found at most maser sites are discussed: (1) excitation by intermediate- or low-mass stars; (2) extremely small UCHII; (3) absorption of UV by dust; and (4) excitation by protostellar or pre–main-sequence objects.

### 4.1. *Excitation by Low-Mass Stars*

The most obvious, but possibly naive, conclusion from this survey is that embedded massive stars are not present at most maser sites. Historically, masers have been considered signposts of massive star formation largely because of their association with H II regions. However this indicates only that massive stars can provide the necessary pump energy, but it does not imply that they are the only stars that can. Masers cannot be associated with all low-mass stars or there would be far more maser sites than are observed. A lower mass limit can be estimated from the statistics of this survey. For a particular initial mass function (IMF), the number of stars within a given mass interval can be calculated. Using only the slope of the IMF, the ratio of stars in two mass intervals can be obtained. If we assume that all the H II regions detected (29) represent stars with mass between $M_2$ and $M_3$, and all maser sites without H II regions (28) represent stars in the interval $M_1$ to $M_2$, we can calculate $M_1$, the lower mass limit required to account for maser sites without H II regions. For an IMF with slope $-2$ and an upper mass limit $M_3 = 100\ M_\odot$, the ratio of stars in the mass intervals $M_1$–$M_2$ and $M_2$–100 is $(M_2/M_1 - 1)/(1 - M_2/100)$. Setting this ratio equal to 28/29 and choosing $M_2 = 17$ (B1 star), we get $M_1 = 9.4\ M_\odot$.

Thus it is not necessary to invoke excitation by very low mass stars in order to account for the detection statistics. In fact, water masers are known to occur near low-mass T-Tauri stars with energetic outflows, so it may be that some of the isolated $H_2O$ masers in our sample are excited by such stars. We regard this as a possible explanation for the lower detection rate of continuum sources toward isolated $H_2O$ masers. This might also help explain the larger number of $H_2O$ masers compared to OH masers found by FC89 (in the ratio $\sim 3/2$). On the other hand, isolated $H_2O$ masers are often located at the centers of massive molecular cores, and $CH_3OH$ masers associated with them can be quite luminous.

For OH masers however, stars of spectral type later than B1 may not be bright enough to account for the OH luminosities. While a collisional pump is accepted for 1.3 cm $H_2O$ masers, an FIR radiative pump is preferred for main-line 18 cm OH masers. For small OH maser groups located at some distance from a central source of luminosity, geometric dilution of the radiation field is large. Balancing the number of OH maser and FIR pump photons can be difficult (Norris & Booth 1981; Elitzur 1992), and luminous sources with low dilution factors are required to account for the observed OH maser brightness temperatures (Pavlakis & Kylafis 1996). If the FIR intensity at OH maser sites is proportional to the stellar luminosity, the number of pump photons available from a B2 star would be 2 orders of magnitude less than from an O5 star. Thus OH maser activity may be difficult to reconcile with an embedded star of low to intermediate stellar mass. Of the 29 maser sites containing OH masers in our sample, 15 (52%) have detected continuum sources. If all OH maser sites do in fact contain embedded massive stars, the lack of continuum emission may indicate an earlier evolutionary phase for these sites. In this case, the nearly equal numbers of OH sites with and without H II regions implies a similar lifetime for OH masers during the phase preceding and the phase following the appearance of UCHIIs.

It can also be shown that external excitation of OH masers is unlikely. Within the molecular envelope surrounding a massive star, the FIR photon rate is sufficient to pump the masers, provided the luminosity comes from a central embedded source. If the IR radiation comes from a source located outside of the envelope, the large dilution factor reduces the local FIR field below that necessary to account for the OH luminosity. An external source of excitation for OH masers is therefore untenable for radiative pumping schemes. In the following discussion the implications of the low UCHII detection rate are examined under

the assumption that the maser sites contain an embedded massive star or protostar. This assumption is consistent with the generally high IR flux density measured toward maser sites and their association with massive molecular cores.

### 4.2. *Extremely Small UCHIIs*

In order to use the observational results quantitatively we need to calculate the expected radio flux density from an H II region produced by an embedded ZAMS star. The spectral type and luminosity class of the star determines the number of photons ($N$ s$^{-1}$) produced that are capable of ionizing hydrogen. The usual source for this relationship is Panagia (1973). More recent calculations including non-LTE effects, line blanketing, and stellar winds (Schaerer & de Koter 1997), which give slightly lower ionizing fluxes than previous derivations, have also been carried out. Under the assumptions of uniform hydrogen density and low optical depth, the total flux density ($S$ mJy) depends on the distance ($D$ kpc), the electron temperature ($T_4$ in units of $10^4$ K), the frequency ($\nu$ GHz), and $f$, the fraction of ionizing photons absorbed by dust:

$$S = \frac{N(1-f)}{7.54 \times 10^{43} \nu^{0.1} T_4^{-0.45} D^2} \text{ mJy} . \quad (1)$$

For $f = 0$, $T_4 = 1$, $D = 5$, $\nu = 8.5$, and $S = 1$, we find $\log N = 45.37$. According to Panagia (1973) this corresponds to a ZAMS star of spectral type B1. At a distance of 1 kpc the number of ionizing photons required to produce a 1 mJy radio source is a factor 25 lower, corresponding to a main-sequence star of spectral type B3.

Using the 3 cm total flux density from Table 1, a spectral type can be derived for each continuum source detected. 23 of the 29 UCHIIs listed have spectral types between O9.5 and B0.5. Only two stars have earlier spectral types (O7 and O8) and two have later types (B1 and B2). The approximate location of the stellar types is shown on the adjusted total flux histogram in Figure 2. The effect of using a Galactic center distance of 8.5 kpc is to reduce the inferred stellar UV fluxes by $\sim$30%. For the brighter stars this is about one spectral subclass, and for B stars it is less than a luminosity class. Figures 2 and 3 remain unchanged except that the reference distance is 4.25 kpc instead of 5 kpc.

Another useful formula (adapted from Garay et al. 1985) is the flux density ($S$ Jy) of a homogeneous H II region as a function of temperature ($T_e$ K), density ($N_e$ cm$^{-3}$), radius ($R$ pc), and distance ($D$ kpc):

$$S = S_{\rm bb}(1 - e^{-\tau}) , \quad (2)$$

where

$$S_{\rm bb} = 9.64 \times 10^2 \nu^2 T_e R^2 D^{-2} \quad (3)$$

and

$$\tau = 4.35 \times 10^{-7} \nu^{-2.1} N_e^2 R T_e^{-1.35} . \quad (4)$$

Using this formula we can derive the size of the H II region required to produce 1 mJy of free-free emission at 8.5 GHz for a given electron temperature and density. The UCHII radius versus $N_e$ is shown in Figure 3 for a distance of 5 kpc and three choices of electron temperature. It can be seen that changing the electron temperature does not have a strong effect. A homogeneous, spherical H II region that lies

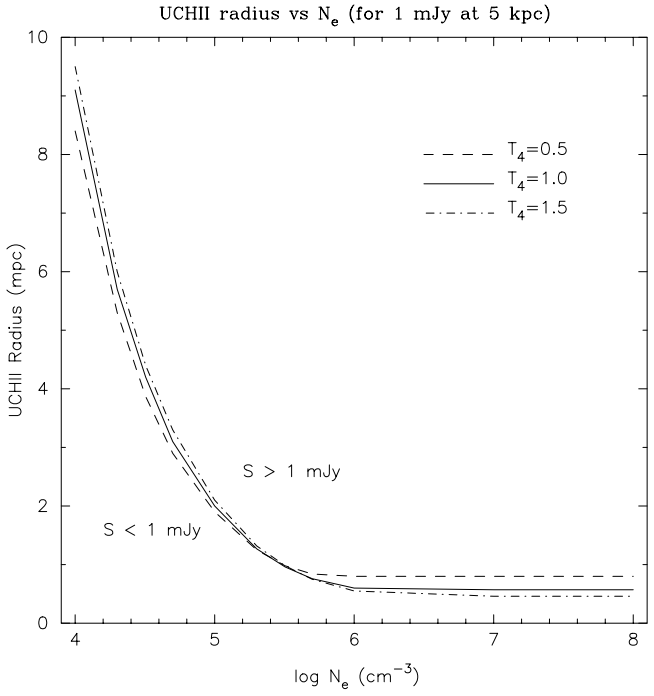


FIG. 3.—UCHII radius required to produce a flux density of 1 mJy at 8.5 GHz for a distance of 5 kpc vs. electron density. Three values of the electron temperature ($T_4$ in units of $10^4$ K) are shown. For combinations of radius and electron density below the curves, the flux density is less than 1 mJy.

in the region above the curve falls within our detection limit. For $N_e \gtrsim 10^{5.5}$ cm$^{-3}$ the H II region becomes optically thick and the radius tends to the 1 mJy blackbody limit. In the optically thick case the number of stellar UV photons needed to account for the measured radio flux density is underestimated; i.e., a spectral type earlier than indicated by equation (1) is required. If UV photons are absorbed by dust ($f > 0$) a similar situation holds.

If all maser sources contain embedded stars of spectral type B1 or earlier, then the 28 maser sites in our survey without continuum detections must have H II regions that lie in the region below the curves in Figure 3. In order to formally assess whether this is reasonable or not, we need to model the temporal and spatial development of a UCHII around an embedded massive star. This requires knowing the evolution of the radiation field at the stellar photosphere, the distribution of dust and gas in the molecular envelope, and the geometry and kinematics of the ionized zone. We also need to know at what point maser emission arises and how long it lasts. Unfortunately we have only limited knowledge of these processes for massive stars, so only plausibility arguments based on a simple geometry can be given.

Assuming that an H II region has formed, Figure 3 indicates that the largest H II region consistent with our 1 mJy limit has a maximum radius of $\sim$2 mpc for an electron density of $10^5$ cm$^{-3}$. Densities below $10^5$ cm$^{-3}$ are unlikely in the molecular cores in which massive stars form; recent molecular line measurements indicate $H_2$ densities of $10^6$–$10^7$ cm$^{-3}$ in such regions (Cesaroni et al. 1994; Akeson & Carlstrom 1996). De Pree, Rodriguez, & Goss (1995) list 10 UCHIIs embedded in molecular gas with ambient densities greater than $10^7$ cm$^{-3}$. At these densities the H II

region is optically thick and the maximum size consistent with the continuum data is $\sim 0.5$ mpc.

The dynamical age of a 2 mpc radius H II region with an expansion velocity of 10 km $s^{-1}$ (the approximate sound speed for a $10^4$ K gas) is 200 yr. Such short dynamical lifetimes were first pointed out for W3(OH) by Dreher & Welch (1981). Since then there have been many theories proposed for extending the lifetime of UCHIIs (e.g., Hollenbach et al. 1994; Dyson, Williams, & Redman 1995; De Pree et al. 1995; Xie et al. 1996). These theories are capable of maintaining UCHII radii at values below 0.1 pc for $\sim 10^5$ yr by employing various sources of external pressure or mass loading. In order to account for the large number of maser sources without detectable H II regions however, a mechanism that keeps the H II radius below $\sim 1$ mpc ($3 \times 10^{15}$ cm) for times comparable to the maser lifetime, which is estimated to be $\sim 10^5$ yr (Genzel & Downes 1977; FC89), is needed.

The simplest model for restricting the size of H II regions is that of De Pree et al. (1995). These authors point out that the radius of an expanding H II region in a constant density environment is determined by the value of the initial Strömgren radius $R_i$, which varies with density as $n^{-2/3}$. The radius increases with time as $R(t) = R_i(1 + 7Vt/4R_i)^{4/7}$, where $V$ is the expansion velocity. For an electron temperature of $10^4$ K, $R_i = 0.675(N_{46}/n_6^2)^{1/3}$ mpc, where $N_{46}$ is the number of ionizing photons produced by the star in units of $10^{46}$ $s^{-1}$ and $n_6$ is the density in units of $10^6$ $cm^{-3}$. The number of ionizing photons is $10^{49}$ for an O6 star and $10^{45.7}$ for a B1 star (Panagia 1973), so assuming $n = 10^7$ we calculate initial Strömgren radii of 1.45 mpc and 0.12 mpc for these stars. After $10^5$ yr of expansion at 10 km $s^{-1}$ the respective H II regions reach radii of 85 and 29 mpc. If dust is present within the ionized zone the initial Strömgren radius is reduced by $(1 - f)^{1/3}$ (Akeson & Carlstrom 1996). For $f = 0.9$ (90% of the stellar UV flux is absorbed) the H II radius after $10^5$ yr is about 60 mpc for the O6 star and 20 mpc for the B1 star. Since the final size of the H II region scales as $n^{-2/7}$ and $t^{4/7}$, a factor 100 reduction in the radius requires a density of $10^{14}$ $cm^{-3}$ or an expansion time of 30 yr. This model thus produces too large an H II region to account for the nondetections, even with substantial dust absorption.

The above model assumes that throughout the expansion phase, the shock and ionization fronts travel at the same velocity. This is true only as long as the internal pressure of the H II region is much greater than the external pressure. Akeson & Carlstrom (1996) show that the final size of an H II region is substantially reduced if the external pressure is taken into account. For an O6 star with $N = 1.2 \times 10^{49}$ embedded in a medium of density $10^7$ $cm^{-3}$ and temperature 100 K, the final H II radius after $10^5$ yr is 25 mpc, a factor 3.4 smaller than the radius calculated using the De Pree model. For isothermal expansion ($T_e = 10^4$ K) in a 100 K gas, the pressure difference at time $t$ is $100[R_i/R(t)]^3$ if the initially ionized mass is conserved. Therefore, external pressure becomes comparable to the internal pressure at a radius $R \sim 5R_i$. For the O6 star this takes a few thousand years, and for the B1 star only a few hundred. Thus external thermal pressure can reduce the H II region size by a factor of $\sim 3$ over the standard model after $\sim 10^4$ yr. The combination of substantial dust absorption and external pressure may suffice to keep the H II region around a B1 star smaller than 1 mpc on timescales of $10^4$ yr, but not $10^5$ yr.

### 4.3. *Dust Absorption*

The presence of dust was seen (§ 4.2) not to have a profound effect on the size of an H II region owing to its $(1 - f)^{1/3}$ dependence. However, the radio flux density varies as $(1 - f)^1$, so for $f = 0.9$ only 10% of the total radio flux for a particular spectral type is produced. The results of the above discussion still hold except that the embedded star has a spectral type equivalent to $N' = N(1 - f)^{-1}$, where $N$ is the number of Lyman photons required to produce the observed radio flux density. For $f = 0.9$ this is equivalent to about one spectral subclass for B stars and to approximately three subclasses for O stars. Thus the minimum mass for embedded stars calculated from the UCHII detection statistics is raised considerably if 90% or more of the stellar UV flux is absorbed by dust.

In order for absorption by dust to explain the low continuum levels measured toward most maser sites, the dust must survive within the ionized zone for periods approaching the maser lifetime. Faison et al. (1998) fit dust cocoon models for 10 Galactic UCHIIs whose spectral energy distributions between 1 mm and 1 $\mu$m are known. Many of these sources have associated $OH/H_2O$ masers. Their results indicate that dust is absent within a radius of 3–18 mpc around the central star. Since the dust sublimation radius is much less than the radius of the cavity, dust within the cavity has either been destroyed by photoevaporation (Storzer & Hollenbach 1999) and/or sputtering (Draine 1995), or it has been evacuated by radiation pressure and/or stellar winds. These UCHIIs may be quite young however, and probably represent the final stage of $OH/H_2O$ maser emission (FC89). The dynamical age of one of them (G5.89 − 0.39) has been directly measured by proper motion studies and is estimated to be about 600 yr old (Acord, Churchwell, & Wood 1998). A similar age was found for W3(OH) by Dreher & Welch (1981).

Since dust melts at temperatures between 1500 and 2000 K and is subject to several disruptive processes, survival of the dust for $10^5$ yr within a few mpc of an OB-type star could be a problem. However, if dust near the photosphere does survive and the internal pressure is insufficient to evacuate the region on these timescales, dust absorption could account for the low continuum levels measured. If the dust is distributed in an accretion disk rather than a shell it may survive much longer. Stellar UV radiation would then escape mainly along the disk axis and could give rise to detectable radio emission. In this case a jetlike morphology and radially decreasing ionized density is expected, producing a weak radio source with spectral index $\alpha \simeq 0.6$. Recent radio continuum studies toward molecular outflow sources provide strong evidence for this morphology (Tofani et al. 1995; Torrelles et al. 1997, 1998; Marti et al. 1999). As pointed out by Hofner et al. (1999), if the ionization is provided by stellar photons rather than shock energy, only the fraction of UV photons radiated along the disk axis contributes to the radio emission. While there is no evidence of a spectral index peak near 0.6 in the continuum sources detected in our survey, this scenario could account for some of the nondetections, especially among the isolated $H_2O$ maser sites.

### 4.4. *Excitation by Pre–Main-Sequence Objects*

So far we have assumed that masers are excited by an embedded star that has reached the ZAMS evolutionary stage. Models of protostellar evolution that include accre-

tion have recently been developed for massive stars (Bernasconi & Maeder 1996). According to the models accretion times exceeding $10^6$ yr are expected for stars in the mass range 15–120 $M_\odot$. In the late pre–main-sequence stage the luminosity comes mainly from gravitational contraction of the core and nuclear burning of deuterium and hydrogen. In the earlier stages the luminosity is dominated by the kinetic energy of accretion, which is released at a shock boundary. The accretion shock energy can be estimated as $L_s \sim \dot{M}GM/R$, where $M$ and $R$ are the core mass and radius and $\dot{M}$ is the core accretion rate (Appenzeller, Lequeux, & Silk 1980). Recent theory (Stahler, Pella, & Ho 2000) suggests that infall rates are independent of density and can be estimated by $\dot{M} \sim a^3/G$, where $a$ is the sound speed. For a temperature of 10 K $\dot{M}$ is $\sim 10^{-6}\ M_\odot\ \mathrm{yr}^{-1}$, while at 100 K it is $\sim 4 \times 10^{-5}\ M_\odot\ \mathrm{yr}^{-1}$. Using this relation in the expression for the shock energy we find $L_s \sim 1.6 \times 10^{29} T^{3/2} M_c/R_c$ ergs $\mathrm{s}^{-1}$, where $M_c$ is the core mass in units of $M_\odot$ and $R_c$ is the core radius in mpc. With $T = 10$ K and $M = 10\ M_\odot$, the accretion energy is $\sim 5 \times 10^{31}$ ergs $\mathrm{s}^{-1}$. The total luminosity of water maser emission is $L_w \sim 10^{26} S\ \Delta V\ (\Omega/4\pi) D^2$, where $S$ is the $H_2O$ flux density in Jy, $\Delta V$ is the maser line width in km $\mathrm{s}^{-1}$, $\Omega$ is the beaming angle, and $D$ the distance in kpc. Using 10 Jy and 20 km $\mathrm{s}^{-1}$ as a typical flux density and velocity extent for Galactic $H_2O$ masers (Forster & Caswell 1999) and assuming isotropic maser emission, the water maser luminosity at 5 kpc distance is $L_w \sim 5 \times 10^{29}$ ergs $\mathrm{s}^{-1}$. Since this is 2 orders of magnitude less than the shock energy for a 10 $M_\odot$ core, it appears energetically feasible that water masers could be powered by protostellar accretion shocks. Since the total luminosity of OH masers is typically an order of magnitude less than $H_2O$ masers, protostellar shocks could also power OH masers. However, if the OH masers are radiatively pumped, the shock energy must first be converted into FIR radiation.

Unlike low-mass stars, which do not reach hydrogen fusion temperatures until they reach the ZAMS, massive stars begin nuclear burning in their cores while still accumulating mass. At a core mass of about 10 $M_\odot$ the luminosity of the star rises dramatically as hydrogen burning begins. Under stationary conditions an ionization front advances rapidly when hydrogen ignites and UV photons become abundant. However, at a sufficiently high accretion rate infalling neutral material will use up all the photons at the photosphere and stop the advance. This is similar to mass-loading processes proposed for extending the lifetime of UCHIIs (e.g., Hollenbach et al. 1994; Dyson et al. 1995) but differs in that it stops even the initial development of an H II region. In this way H II radii around even massive stars could be kept below the detection limits for as long as the infall lasts, which may be on the order of $10^6$ yr for massive stars. Walmsley (1995) calculates critical accretion rates of $10^{-4}\ M_\odot\ \mathrm{yr}^{-1}$ for a 60 $M_\odot$ O5 star and $4 \times 10^{-6}\ M_\odot\ \mathrm{yr}^{-1}$ for a 17 $M_\odot$ B1 star. These appear to be reasonable infall rates, amounting to an accumulation of 10 $M_\odot$ in $10^5$ yr for the O5 star.

## 5. SUMMARY AND CONCLUSIONS

Images of the 3 cm continuum emission toward 26 star-forming regions containing both OH and $H_2O$ masers have been obtained with an rms sensitivity of $\sim$0.15 mJy. Of a total of 45 individual maser sites in these regions, compact continuum emission was detected at 17 sites, giving an overall detection rate of 38%. If restricted to sites containing OH maser emission, the detection rate is about 50%. For sites containing $H_2O$ masers the rate is 33%, and for isolated $H_2O$ maser sites without associated OH emission the rate is 13%.

The total number of compact continuum sources detected in all fields combined is 29. The spectral index distribution of these sources peaks between 0 and 0.2, with most of the maser sources having indices less than 1.0. There is no evidence in our data for a peak near 0.6, which would indicate that the continuum emission is due to an ionized stellar wind rather than a homogeneous H II region. Adjusted to a standard distance of 5 kpc, we find that most UCHIIs have total flux densities $\lesssim$100 mJy and radii $\lesssim 1''$ (24 mpc). Most of the smaller and weaker sources have associated maser emission.

The survey statistics were discussed under the assumption that each maser site contains an embedded star and that any continuum emission comes from a UCHII surrounding the star. If the exciting sources are ZAMS stars of spectral type B1 or earlier, the common absence of detectable continuum emission requires that the H II region remain smaller than about 1 mpc for the duration of the maser phase ($\sim 10^5$ yr). Dynamical models that include the effects of dust absorption and external pressure in a hot (100 K) and dense ($10^7$ $\mathrm{cm}^{-3}$) medium are capable of keeping the radius of an H II region below 1 mpc on timescales of $\sim 10^4$ yr, but not for durations of $10^5$ yr. Heavy absorption of UV photons in a spherical dust shell could reduce the continuum emission to the measured levels, but it is not clear that dust could survive that long within a few mpc of the stellar photosphere.

We conclude that the presence of an embedded ZAMS star of spectral type B1 or earlier is inconsistent with the continuum flux density levels measured (in particular, the upper limits) for most of the maser sites in our survey if the masers last for $10^5$ yr. While it is possible that some of the isolated $H_2O$ masers may be excited by low-mass stars, we find that a lower mass limit of about 10 $M_\odot$ for the embedded stars can account for the detection statistics. The possibility that stars of intermediate mass (10–17 $M_\odot$) are responsible for about half of the known interstellar masers appears feasible. However, there may be an energy balance problem for OH maser sites that are pumped by FIR photons. Excitation of collisionally excited masers by lower mass stars is possible and perhaps even likely for weak, isolated $H_2O$ masers. These sites would be characterized by a low core mass and luminosity.

Excitation of maser emission in the envelopes of accreting massive protostars is found to be energetically feasible. Since accretion timescales of order $10^6$ yr are predicted by recent models, accounting for maser lifetimes of $10^5$ yr is not a problem. The eventual formation of a UCHII is inevitable in this case, although at sufficiently high accretion rates development of the H II region would be severely retarded. Distribution of infalling material in an accretion disk would allow the development of a weak continuum source along the polar axis, which would eventually evolve into a UCHII. Such maser sites would be characterized by high core mass and luminosity, broad molecular line emission, and infall in their early stages, with outflows, stellar winds, and H II regions toward the end of their lifetime.

The majority of interstellar OH/$H_2O$ masers in the Galaxy are clearly associated with sites of massive star for-

mation. Although masers disappear in the later stages of development of an H II region, they are present at the earliest detectable stage and could be present even earlier. Although we are not yet able to make an unequivocal choice among the various possibilities considered to account for the lack of strong continuum emission at many maser sites, we regard the earlier evolutionary phase option as the most attractive. The question of whether maser sites without H II regions might be excited by lower mass stars can be resolved only by measuring the luminosity of the embedded YSO. Such measurements should be made near the wavelength of maximum emission in order to avoid a large extrapolation and will become possible with the development of high-resolution telescopes in the submillimeter and far-infrared. It would be especially valuable to study maser sites with weak centimeter $\lambda$ continuum sources in order to improve our understanding of the effects of mass and evolution in these young star-forming regions.

We thank Robin Wark for help with the observations and Bob Sault for consultations on data reduction using MIRIAD. We are grateful for many helpful comments by an anonymous referee, which substantially improved the manuscript. The Australia Telescope is funded by the Commonwealth of Australia for operation as a National Facility managed by CSIRO.

## REFERENCES

Acord, J. M., Churchwell, E., & Wood, D. O. S. 1998, ApJ, 495, L107
Akeson, R. L., & Carlstrom, J. E. 1996, ApJ, 470, 528
Appenzeller, I., Lequeux, J., & Silk, J. 1980, Star Formation—10th Advanced Course, ed. A. Maeder & L. Martinet (Geneva: Geneva Obs. Publ.), 34
Baart, E. E., & Cohen, R. J. 1985, MNRAS, 213, 641
Becker, R. H., White, R. L., Helfand, D. J., & Zoonematkermani, S. 1994, ApJS, 91, 347
Bernasconi, P. A., & Maeder, A. 1996, A&A, 307, 829
Carral, P., Kurtz, S., Rodriguez, L. F., Marti, J., Lizano, S., & Osorio, M. 1999, Rev. Mexicana Astron. Astrofis., 35, 97
Caswell, J. L. 1997, MNRAS, 289, 203 (C97)
———. 1998, MNRAS, 297, 215
Caswell, J. L., Vaile, R. A., & Forster, J. R. 1995, MNRAS, 277, 210
Cesaroni, R., Churchwell, E., Hofner, P., Walmsley, C. M., & Kurtz, S. 1994, A&A, 288, 903
Churchwell, E., Walmsley, C. M., & Cesaroni, R. 1990, A&AS, 83, 119
Codella, C., Felli, M., & Natale, V. 1996, A&A, 311, 971
Codella, C., Felli, M., Natale, V., Palagi, F., & Palla, F. 1994, A&A, 291, 261
Codella, C., Testi, L., & Cesaroni, R. 1997, A&A, 325, 282
Cook, A. H. 1968, MNRAS, 140, 299
De Pree, C. G., Rodriguez, L. F., & Goss, W. M. 1995, Rev. Mexicana Astron. Astrofis., 31, 39
Draine, B. T. 1995, Ap&SS, 233, 111
Dreher, J. W., & Welch, W. J. 1981, ApJ, 245, 857
Dyson, J. E., Williams, R. J. R., & Redman, M. P. 1995, MNRAS, 277, 700
Elitzur, M. 1992, ARA&A, 30, 75
Elitzur, M., & de Jong, T. 1978, A&A, 67, 323
Ellingsen, S. P., Norris, R. P., & McCulloch, P. M. 1996, MNRAS, 279, 101
Faison, M., Churchwell, E., Hofner, P., Hackwell, J., Lynch, D. K., & Russell, R. W. 1998, ApJ, 500, 280
Forster, J. R., & Caswell, J. L. 1989, A&A, 213, 339 (FC89)
———. 1999, A&AS, 137, 43
Garay, G., Moran, J. M., Rodriguez, L. F., & Reid, M. J. 1998, ApJ, 492, 635
Garay, G., Reid, M. J., & Moran, J. M. 1985, ApJ, 289, 681
Gaume, R. A., & Mutel, R. L. 1987, ApJS, 65, 193
Genzel, R., & Downes, D. 1977, A&AS, 30, 145
Ho, P. T. P., & Haschick, A. D. 1981, ApJ, 248, 622
Hofner, P., Kurtz, S., Churchwell, E., Walmsley, C. M., & Cesaroni, R. 1994, ApJ, 429, L85
———. 1996, ApJ, 460, 359
Hofner, P., Cesaroni, R., Rodriguez, L. F., & Marti, J. 1999, A&A, 345, L43
Hofner, P., & Churchwell, E. 1996, A&AS, 120, 283
Hollenbach, D., Johnstone, D., Lizano, S., & Shu, F. 1994, ApJ, 428, 654
Kerr, F. J., & Lynden-Bell, D. 1986, MNRAS, 221, 1023
Marti, J., Rodriguez, L. F., & Torrelles, J. M. 1999, A&A, 345, L5
Mezger, P. G., & Robinson, B. J. 1968, Nature, 220, 1107
Norris, R. P., & Booth, R. S. 1981, MNRAS, 195, 213
Panagia, N. 1973, AJ, 78, 929
Pavlakis, K. G., & Kylafis, N. D. 1996, ApJ, 467, 309
Sault, R. J., Teuben, P. J., & Wright, M. C. H. 1995, in ASP Conf. Ser. 77, Astronomical Data Analysis Software and Systems IV, ed. R. A. Shaw, H. E. Payne, & J. J. E. Hayes (San Francisco: ASP), 433
Schaerer, D., & de Koter, A. 1997, A&A, 322, 598
Stahler, S. W., Palla, F., & Ho, P. T. P. 2000, in Protostars and Planets IV, ed. V. Mannings, A. P. Boss, & S. S. Russel (Tucson: Univ. Arizona Press), in press
Storzer, H., & Hollenbach, D. 1999, ApJ, 515, 669
Tarter, J. C., & Welch, W. J. 1986, ApJ, 305, 467
Tofani, G., Felli, M., Taylor, G. B., & Hunter, T. R. 1995, A&AS, 112, 299
Torrelles, J. M., Gomez, J. F., Garay, G., Rodriguez, L. F., Curiel, S., Cohen, R. J., & Ho, P. T. P. 1998, ApJ, 509, 262
Torrelles, J. M., Gomez, J. F., Rodriguez, L. F., Ho, P. T. P., Curiel, S., & Vazquez, R. 1997, ApJ, 489, 744
Turner, J. L., & Welch, W. J. 1984, ApJ, 287, L81
Walmsley, M. 1995, Rev. Mexicana Astron. Astrofis., 1, 137
Weaver, H., Williams, D. R. W., Dieter, N. H., & Lum, W. T. 1965, Nature, 208, 29
Wood, D. O. S., & Churchwell, E. 1989, ApJS, 69, 831
Xie, T., Mundy, L. G., Vogel, S. N., & Hofner, P. 1996, ApJ, 473, L131